Climate Dynamics (2018) 51:3179–3193
https://doi.org/10.1007/s00382-018-4073-y

Time of emergence in regional precipitation changes: an updated assessment using the CMIP5 multi-model ensemble

Thuy-Huong Nguyen[1,2] · Seung-Ki Min[1] · Seungmok Paik[1] · Donghyun Lee[1]

Received: 2 July 2017 / Accepted: 1 January 2018 / Published online: 17 January 2018

Abstract
This study conducted an updated time of emergence (ToE) analysis of regional precipitation changes over land regions across the globe using multiple climate models from the Coupled Model Intercomparison Project phase 5 (CMIP5). ToEs were estimated for 14 selected hotspots over two seasons of April to September (AS) and October to March (OM) from three RCP scenarios representing low (RCP2.6), medium (RCP4.5), and high (RCP8.5) emissions. Results from the RCP8.5 scenario indicate that ToEs would occur before 2040 over seven hotspots including three northern high-latitude regions (OM wettening), East Africa (OM wettening), South Asia (AS wettening), East Asia (AS wettening) and South Africa (AS drying). The Mediterranean (both OM and AS drying) is expected to experience ToEs in the mid-twenty-first century (2040-2080). In order to measure possible benefits from taking low-emission scenarios, ToE differences were examined between the RCP2.6 scenario and the RCP4.5 and RCP8.5 scenarios. Significant ToE delays from 26 years to longer than 67 years were identified over East Africa (OM wettening), the Mediterranean (both AS and OM drying), South Asia (AS wettening), and South Africa (AS drying). Further, we investigated ToE differences between CMIP3-based and CMIP5-based models using the same number of models for the comparable scenario pairs (SRESA2 vs. RCP8.5, and SRESB1 vs. RCP4.5). Results were largely consistent between two model groups, indicating the robustness of ToE results. Considerable differences in ToEs (larger than 20 years) between two model groups appeared over East Asia and South Asia (AS wettening) and South Africa (AS drying), which were found due to stronger signals in CMIP5 models. Our results provide useful information on the timing of emerging signals in regional and seasonal hydrological changes, having important implications for associated adaptation and mitigation plans.

Keywords Time of emergence · Precipitation · CMIP5 · RCP scenarios · Signal-to-noise ratio

1 Introduction

"Time of emergence" (ToE) indicates when a climate change signal emerges clearly from the background noise of natural variability (Christensen et al. 2007; Giorgi and Bi 2009; Hawkins and Sutton 2011, 2012; Bindoff et al. 2013; Maraun 2013; Sui et al. 2014; King et al. 2015; Lee et al. 2016). ToE provides useful information for end users on adaptation planning and mitigation strategies. Analysis of the signal-to-noise ratio is one of the main approaches to detect the ToE of a climate signal based on climate models. The signal of future precipitation change can be calculated based on individual models (e.g., Hawkins and Sutton 2012; Maraun 2013; Sui et al. 2014) or multi-model ensembles (e.g., Christensen et al. 2007; Giorgi and Bi 2009; Hawkins and Sutton 2011). The advantages of using multi-model ensembles is that the errors related to model biases can be reduced by taking multi-model means (Lambert and Boer 2001; Min et al. 2004; Phillips and Gleckler 2006); if projection biases have Gaussian/Normal distribution, then negative and positive values can be averaged out to better represent future precipitation projections. In fact, models are diverse, and a model can provide a good projection for a specific area, period and variable, but not always for all cases (Lambert and Boer 2001). Different assumptions on emission scenarios, initial inputs, and physical feedback

✉ Seung-Ki Min
skmin@postech.ac.kr

[1] Division of Environmental Science and Engineering, Pohang University of Science and Technology, 77 Cheongam-ro Nam-gu, Pohang, Gyeongbuk 37673, Korea

[2] Present Address: REMOSAT Laboratory, University of Science and Technology of Hanoi, Hanoi, Vietnam

processes cause different model projections. In this regard, using multi-model ensembles also provide an advantage of quantifying the uncertainty in future projections into different sources of uncertainty, such as internal variability, inter-model uncertainty, and scenario uncertainty (Giorgi and Bi 2009; Giorgi 2010; Hawkins and Sutton 2011, 2012).

Although temperature shows smooth changes with a positive sign over the most regions from external forcing, precipitation change is different from region to region. Although anthropogenic influence on the observed precipitation change has been detected in some regions, such as the northern high-latitudes (Min et al. 2008; Noake et al. 2012; Wan et al. 2015), detecting precipitation change signals is more difficult than temperature changes due to relatively small signal-to-noise ratio (Räisänen 2001; Hawkins and Sutton 2011; Mora et al. 2013; Sarojini et al. 2016). Despite the large uncertainty, a reliable estimate of ToE for precipitation is fundamentally required for making necessary adaptation plans on regional scales. Previous studies assessed ToE for precipitation changes on different spatial scales (global, continental, and regional) using Global Climate Models (GCMs) (Giorgi and Bi 2009; Hawkins and Sutton 2011; Mora et al. 2013; Sui et al. 2014; King et al. 2015) or Regional Climate Models (RCMs) (Maraun 2013). Giorgi and Bi (2009, hereinafter GB09) identified 14 hotspots of precipitation changes and examined ToEs for three Special Report on Emissions Scenarios (SRES) using the Coupled Model Inter comparison Project phase 3 (CMIP3) multi-model ensemble. They found that six out of 14 hotspots would have ToEs in the early twenty-first century, including northern high-latitude regions, the Mediterranean, and East Africa; East and South Asia and the Caribbean had ToEs in the mid-twenty-first century; and five other regions in the late decades or beyond (based on the SRESB1 scenario).

Future projections of climate change including precipitation will be highly dependent on the emission scenarios. Quantifying benefits of reduced emissions by earlier ToEs is important to inform the timing of the significant climate change. In general, ToE for precipitation change is expected to occur later under more aggressive mitigation scenario than weaker mitigation scenarios (cf. Ciavarella et al. 2017). In this respect, the Representative Concentration Pathways (RCPs) scenarios were newly introduced, which incorporate new socio-economic information, emerging technologies and other factors, such as land use and land-cover change (Moss et al. 2010; van Vuuren et al. 2011; Rogelj et al. 2012). Accordingly, the Coupled Model Intercomparison Project phase 5 (CMIP5) ensemble experiments were carried out under the different RCP scenarios that represent different degree of mitigation efforts.

To the best of our knowledge, there have been no studies that have comprehensively updated the GB09 results to consider ToE delays in regional precipitation changes under the new RCP scenarios. The ToE estimates from the updated scenarios will identify regions that will benefit from emission reduction through ToE delay. Moreover, new scenarios provide a larger number of CMIP5 models and include more completely treated forcing agents with respect to aerosols and land use than the previous model group of CMIP3 (Stocker et al. 2013). Thus, comparing ToE estimates between CMIP3 and CMIP5 ensembles will help to assess robustness of the ToE results. Therefore, in this study, we use multiple climate models from CMIP5 under three RCP scenarios to conduct an updated ToE analysis of regional precipitatiob changes over the 14 hotspot regions. Particular focus is given to the investigation of ToE differences between the RCP scenarios, which will quantify benefits of mitigation through ToE delay.

2 Data and methods

2.1 Scenarios and model simulations

Each scenario introduces a unique projection of radiative forcing and temperature target. The RCP2.6 has a radiative forcing of about 2.6 W m^{-2} in the year 2100 relative to pre-industrial values and CO_2 concentration will be about 490 ppm before 2100; it has a global mean surface air temperature (GMST) increase of about 1.0 °C (5–95% range 0.3–1.7 °C) up to the late twenty-first century with respect to 1986–2005 (Collins et al. 2013). The RCP2.6 is the lowest emission scenario, requiring climate policy to limit emissions. The RCP4.5 has a radiative forcing of about 4.5 W m^{-2} and CO_2 concentration reaches 650 ppm in the twenty-first century but does not increase after that; it has a GMST increase of about 1.8 °C (1.1–2.6 °C) by the late twenty-first century. The RCP4.5 and the SRESB1, the low-emission scenario in CMIP3, are comparable scenarios (van Vuuren et al. 2011). The RCP8.5 has a radiative forcing of 8.5 W m^{-2} in 2100 and a peak of CO_2-equivalent at > 1370 ppm before the year 2100; it has a GMST increase of about 3.7 °C (2.6–4.8 °C). The RCP8.5 and the SRESA2, the high population growth scenario in CMIP3, are considered as business-as-usual scenarios (van Vuuren et al. 2011).

To update ToE results and examine potential ToE delay under the low-emission scenario of RCP2.6, we selected 28 CMIP5 models that are available in historical experiment (HIST), RCP2.6, RCP4.5 and RCP8.5 scenarios. Refer to Table 1 for details. Updated ToE results were also compared with those from CMIP3 model simulations integrated under SRESA2 and SRESB1 scenarios as given in GB09 (Table 2). 20C3M runs were also used, which provide current climate conditions for CMIP3, equivalent to HIST runs of CMIP5.

Here we used two 6-month periods, from April to September (AS)—Northern hemisphere summer, and from

Table 1 List of CMIP5 simulations used in this study

No	MODEL	HIST	RCP2.6	RCP4.5	RCP8.5	TCR
1	bcc-csm1-1	3	1	1	1	1.7
2	bcc-csm1-1-m	3	1	1	1	2.1
3	BNU-ESM	1	1	1	1	2.6
4	CanESM2	5	5	5	5	2.4
5	CCSM4	6	1	6	6	1.8
6	CESM1-CAM5	3	3	3	3	2.3
7	CESM1-WACCM	4	1	1	1	1.8[a]
8	CNRM-CM5	10	1	1	5	2.1
9	CSIRO-Mk3-6-0	10	10	10	10	1.8
10	EC-EARTH	6	2	9	9	2.0[b]
11	FGOALS-g2	1	1	1	1	1.4
12	FIO-ESM	3	3	3	3	–
13	GFDL-CM3	5	1	1	1	2.0
14	GFDL-ESM2G	3	1	1	1	1.1
15	GFDL-ESM2M	1	1	1	1	1.3
16	GISS-E2-H	15	3	15	3	1.7
17	GISS-E2-R	22	3	17	3	1.5
18	HadGEM2-AO	1	1	1	1	2.0[c]
19	HadGEM2-ES	4	4	4	4	2.5
20	IPSL-CM5A-LR	6	4	4	4	1.5
21	MIROC5	5	3	3	3	1.5
22	MIROC-ESM	3	1	1	1	2.2
23	MIROC-ESM-CHEM	1	1	1	1	–
24	MPI-ESM-LR	3	3	3	3	2.0
25	MPI-ESM-MR	3	1	3	1	2.0
26	MRI-CGCM3	5	1	1	1	1.6
27	NorESM1-M	3	1	1	1	1.4
28	NorESM1-ME	1	1	1	1	1.6
Total		136	60	100	76	

TCR value sources: IPCC (2013)

[a]Muthers et al. (2014)

[b]Kjellström et al. (2016)

[c]Mullan et al. (2016)

October to March (OM)—Southern hemisphere summer, to classify climate zone types following GB09. These two 6-month periods include the rainy seasons in most monsoon areas and cover the whole year. Therefore, they are often used for analysis of seasonal precipitation change on continental scales (Peel et al. 2007; Kirtman et al. 2013). For example, seasonal precipitation variation is generally strong at low latitudes, but small at middle or high latitude regions (Flato et al. 2013). Because our study updates ToE results from GB09, we adopted the same 14 precipitation change hotspots (PSPOTs), which include northern high-latitude regions, arid and monsoon regions (Fig. 1; Table 3). Multi-model means of CMIP5 (Fig. 1) produce large-scale patterns of precipitation changes very similar to those from GB09 based on CMIP3 multi-models in most regions. Following GB09, we also used relative change with respect to the present-day climatology for our ToE assessment (see below for details). For better comparison, also following GB09, model simulations and observation datasets were interpolated onto a common $1° \times 1°$ grid prior to analysis, with applying a 1-degree land mask from ERA-Interim (Dee et al. 2011). Results were largely insensitive to the use of different resolution (e.g. $2° \times 2°$ grids) for interpolation (not shown), which seems to be due to the consideration of broad area means in our study, as discussed by GB09.

2.2 ToE analysis

We used the signal-to-noise ratio (S/N) method following GB09 to estimate ToEs. To calculate signals, we first computed the 20-year running mean precipitation for each realization of each model. Then we defined each year's signal as

Table 2 List of CMIP3 simulations used in this study

No	Model	20c3m	SRESA2	SRESB1	TCR
1	cccma-cgcm3-1	5	5	4	1.9
2	cnrm-cm3	1	1	1	1.6
3	csiro-mk3-0	3	1	1	1.4
4	gfdl-cm2-0	3	1	1	1.6
5	giss-model-e-r	9	1	1	1.5
6	inmcm3-0	1	1	1	1.6
7	ipsl-cm4	2	1	1	2.1
8	miroc3-2-medres	3	3	3	2.1
9	miub-echo-g	5	3	3	1.7[a]
10	mpi-echam5	3	3	3	2.2
11	mri-cgcm2-3-2a	5	5	5	2.2
12	ncar-ccsm3-0	8	4	6	1.5
13	ncar-pcm1	4	4	2	1.3
14	ukmo-hadcm3	2	1	1	2.0
Total		54	34	33	

TCR value source: IPCC (2007)

[a]Kuhlbrodt and Gregory (2012)

the ensemble mean percentage change of the 20-year running means relative to each model's ensemble average over the reference period (1980–1999); e.g., the signal of the year 2040 is the relative change between the 20-year ensemble average for 2021–2040 and the model's ensemble average over 1980–1999. Finally, the signal is defined as the arithmetic average across all models including single and multi-realization models. After obtaining the time series of signals, we repeated the same processes to derive noise. GB09 includes two main sources of noise variance: internal-model variance and inter-model variance. We did not evaluate inter-annual variability because the 20-year running mean cancels it out. We calculated internal-model variance to consider the differences within a model for all multi-realization models, and inter-model variance to investigate the difference in model means. Overall noise was calculated by taking the square root of the sum of internal-model variance and inter-model variance. The details are as follows. Signal (S) in % for a given year is calculated using the following formula:

$$S = \frac{1}{m}\sum_{i=1}^{m} x_i, \tag{1}$$

where m is the total number of models, and and x_i is precipitation change (%) in model i, which is defined as

$$x_i = \frac{1}{n_i}\sum_{j=1}^{n_i} x_{ji}. \tag{2}$$

Here x_{ji} is precipitation change (%) in realization j of model i and n_i is the number of realization of model i. Noise (N) for a given year is defined as follows:

$$N = \sqrt{\sigma_{im}^2 + \sigma_{in}^2}, \tag{3}$$

where N is total standard deviation, σ_{im}^2 is inter-model variance (%^{2}) and σ_{in}^2 is internal-model variance (%^{2}), each of which is defined as:

$$\sigma_{im}^2 = \frac{1}{m}\sum_{i=1}^{m}(x_i - S)^2, \tag{4}$$

$$\sigma_{in}^2 = \frac{1}{\sum_{i=1}^{k} n_i}\sum_{i=1}^{k}\left(\sum_{j=1}^{n_i}(x_{ji} - x_i)^2\right). \tag{5}$$

Using S and N calculated for each region and season, the ToE year is defined as the year at which S becomes larger than N (S/N > 1) with the assumption that this condition remains permanent until the end of twenty-first century. This is the same threshold as that used in GB09 to define confidence level of emergence. This means that, starting from ToE, we have a likelihood of emergence of about 84%, which is equivalent to a cumulative probability of less than one standard deviation. Although we calculate ToEs until 2099, ToEs after 2090 are not reliable due to too short period for the permanent emergence. The choice of 2090 as a cut off is later than in most previous studies. However, we use a multi-model ensemble, which smoothes out decadal variability that might be important in individual model runs.

To improve the ToE comparison with the GB09 results obtained from 14 CMIP3 models, we first randomly selected 14 models out of the 28 CMIP5 models without replacement and calculated ToEs. This was repeated 1000 times and 5th–95th percentile ranges and median of ToEs were estimated for comparison with GB09 results. This ToE estimation from random sampling indicates some uncertainty ranges of ToE due to different model samples, as other studies have shown differences in ToE in individual models (e.g., Hawkins et al. 2014; King et al. 2015). In this regard, we further conducted a comparison between ToEs estimated from individual models with those from multi-models (see Sect. 4).

2.3 Sensitivity test

Model climatology bias may or may not affect projections of precipitation change (Giorgi and Coppola 2010). We used observation data from the Climatic Research Unit (CRU.3.21, New et al. 2000) to explore the possible influence of model bias on the precipitation signal and ToE.

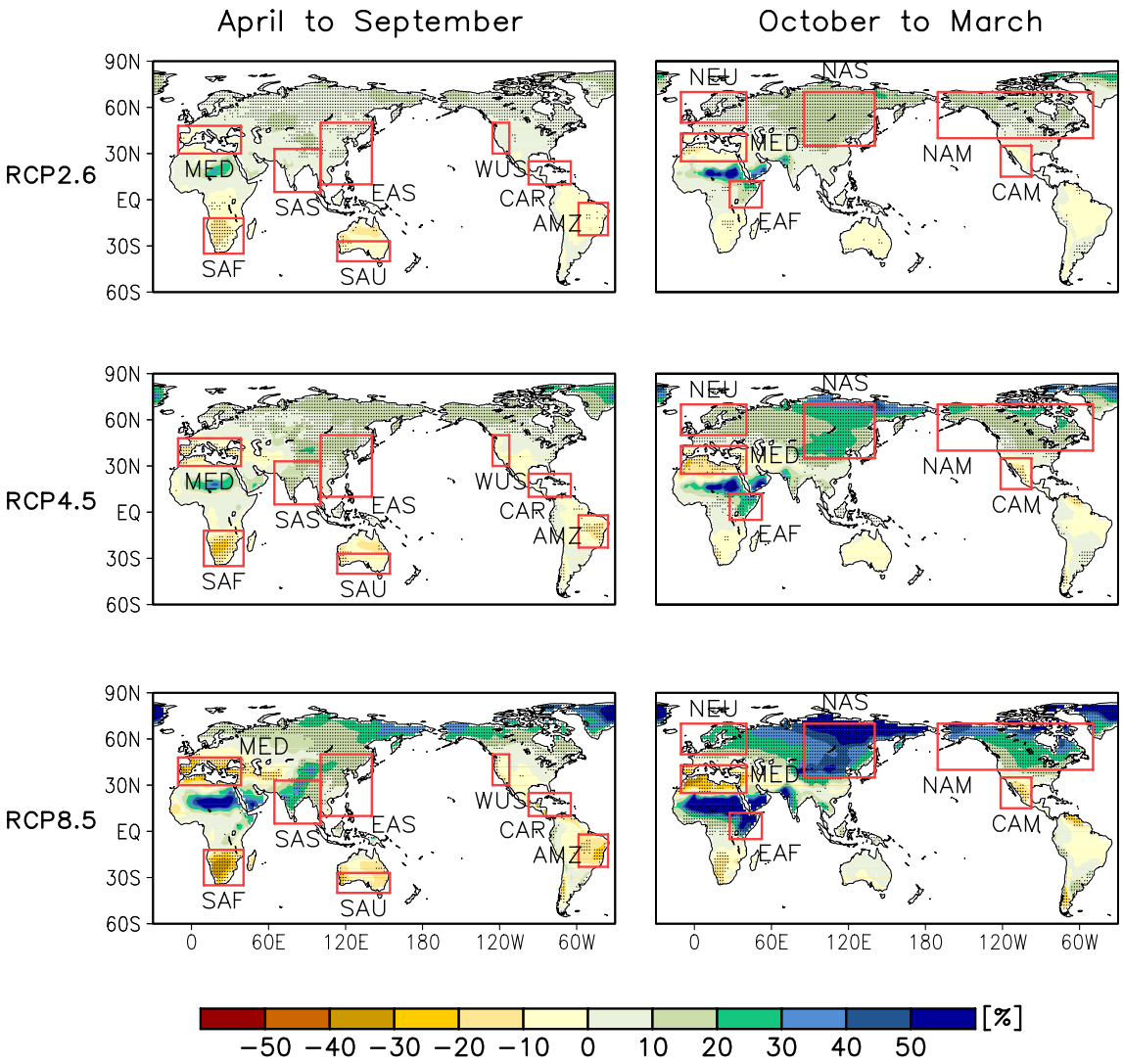

Fig. 1 Patterns of future precipitation change from 28 CMIP5 models. Data are presented as the difference between the two season means for the periods 2080–2099 and 1980–1999 in three RCP scenarios, RCP2.6, RCP4.5, and RCP8.5. Open boxes indicate PSPOTs (land only). Units are % relative to 1980–1999 value. Stippling regions: 80% of models agree on the sign of change

For each region, we examined the inter-model relationship between model bias in precipitation climatology for 20 years (1980–1999) and projected changes in precipitation during the late twenty-first century (2070–2099). It is notable that observations may have uncertainty in precipitation intensity over the land (Herold et al. 2016). However, observational uncertainties would not affect our results much since we focus on the inter-model relationship (between model bias and future projection) rather than absolute values. Because the models' spread in precipitation change may be attributed to the uncertainty in climate sensitivity, we also investigated the relationship between climate sensitivity presented by the Transient Climate Response (TCR; Tables 1, 2) and precipitation change projected by each model.

3 Results

3.1 Precipitation change hotspots

Multi-model mean precipitation changes from CMIP5 28 models show increasing and decreasing patterns in the future (2080–2099) relative to the past (1980–1999) for the two seasons of AS and OM (Fig. 1). PSPOTs have been selected following GB09, which show larger magnitudes of change and greater model agreement on the sign of the change, as in CMIP3 results. During AS, two positive-change hotspots over Asian monsoon regions (EAS and SAS) and six negative-change hotspots (MED, SAF, SAU, WUS, CAR, and AMZ) are identified, whereas four positive-change hotspots over the northern high-latitudes (NAS, NAM, and NEU)

Table 3 Information on 14 PSPOTs

Season	Type	Region	Abbreviation	Latitude	Longitude
Oct–Mar	Drying	Central America	CAM-OM	15N–35N	121.5W–112.5W
		Mediterranean	MED-OM	25N–43N	10.5W–40.5W
	Wettening	Northern Europe	NEU-OM	50N–70N	10.5W–40.5E
		Northern Asia	NAS-OM	35N–70N	85.5W–140.5W
		Northern North America	NAM-OM	40N–70N	170.5W–49.5W
		East Africa	EAF-OM	5S–12N	27.5E–52.5E
Apr–Sept	Wettening	East Asia	EAS-AS	10N–50N	100.5E–140.5E
		South Asia	SAS-AS	5N–33N	64.5E–100.5E
	Drying	Western United State	WUS-AS	30N–50N	125.5W–112.5W
		South Australia	SAU-AS	40S–27S	113.5E–154.5E
		South Africa	SAF-AS	35S–12S	9.5E–40.5E
		Mediterranean	MED-AS	20N–48N	10.5W–38.5W
		Caribbean	CAR-AS	10N–25N	97.5W–64.5W
		Amazon basin	AMZ-AS	23S–2S	58.5W–35.5W

and East Africa (EAF) and two negative-change hotspots (MED and CAM) are identified during OM (Fig. 1). Multi-model mean precipitation changes and inter-model agreement become greatest under the strongest emission scenario of RCP8.5, indicating higher probability of the signal emergence out of the inter-model noise.

The precipitation increase over tropical regions can be explained by a "warmer-get-wetter" theory in which increasing sea surface temperature causes a precipitation increase by the Clausius–Clapeyron relation, and the increased land–ocean temperature contrast increases the amount of moisture transport to the land (Kirtman et al. 2013; Sarojini et al. 2016). The precipitation increase over the northern high-latitude regions is consistent with the observed Arctic moistening (Min et al. 2008; Wan et al. 2015) that is attributable to the pole-ward shift of storm tracks under the greenhouse warming. The drying trend of sub-tropic regions during both seasons can be attributed to the poleward shift of the subtropical dry zones in both hemispheres (Christensen et al. 2007; Kirtman et al. 2013).

Overall precipitation changes over the PSPOTs are consistent with results obtained from CMIP3 in GB09. In both seasons, model agreement on the sign of precipitation change and inter-model variance noise mostly increase as radiative forcing of scenarios is increased (Figs. 1, 2). Model agreement on the sign of the change is largest in northern high-latitudes and smallest in tropics except for two Asian monsoon regions (Fig. 1). Figure 2 shows the inter-model and internal-model variance in the future precipitation changes for 14 PSPOTs averaged for 2080–2099 compared to 1980–1999. The inter-model differences in precipitation changes are higher in tropical regions such as AMZ, CAR, SAU, and EAF. Overall, internal-model variances are much smaller than inter-model variances, indicating the noise dominated by the differences in precipitation projections across models, as found in previous studies (Hawkins and Sutton 2011; King et al. 2015). The precipitation change uncertainty in selected regions, which contains coastline, could be partly due to the different resolution of the models (GB09). Therefore, to estimate ToEs of these regions, we average the precipitation over the areas before calculating signal.

3.2 ToE from CMIP5 models

The inter-model spread of precipitation changes varies over different periods of the twenty-first century and for different scenarios (Fig. 2). Figure 3 illustrates some examples of the time evolution of the signal and noise in the precipitation changes over the six PSPOTs. The signal generally strengthens (increase or decrease in precipitation) over time and in some regions a significant difference in signal exists between scenarios near the end of the twenty-first century. The noise also increases with time, but with different rate of changes across regions. The ToE year is defined as the year at which the signal exceeds the noise permanently as described in Sect. 2. For example, during AS, the signal for drying regions such as the Amazon basin (AMZ) never exceeds noise during the twenty-first century, which means no ToE occurrence (Fig. 3a). In contrast, during OM, the signal over the northern high-latitude regions like northern Asia (NAS) is always greater than noise, and ToEs occur before 2020 (Fig. 3f). This means that the anthropogenic signal in the region is easier to detect than the other regions, consistent with previous studies that found human influence on precipitation increases in the northern high-latitudes during the past several decades (Min et al. 2008; Wan et al. 2015). ToEs

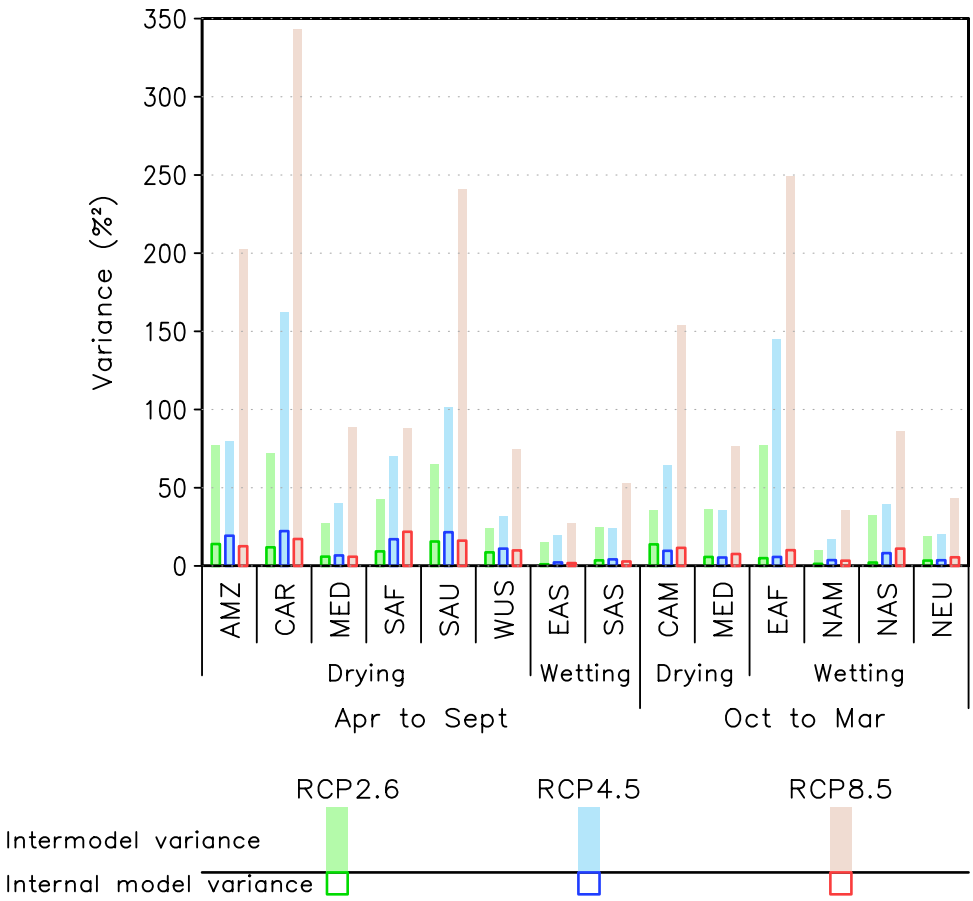

Fig. 2 Inter-model and internal-model variance in future (2080–2099) precipitation changes with respect to the past period (1980–1999) over 14 PSPOTs from RCP2.6 (green), RCP4.5 (blue), and RCP8.5 (red) scenarios

of other regions appear in different periods depending on scenario, such as the Mediterranean (MED) experiencing ToEs in the mid-twenty-first century under RCP8.5 (Fig. 3c), while ToE for East Africa (EAF) appears in the early twenty-first century (Fig. 3d).

Using the same ToE classification as GB09 for early ToE (up to 2040), mid ToE (2040–2080) and late ToE (beyond 2080), we find that, based on the RCP4.5 scenario, early ToEs occur in wettening regions, such as East Asia in AS and northern high-latitude regions in OM; mid ToEs happen in South Asia and South Africa in AS and East Africa in OM; and late ToEs happen in other drying regions (Fig. 4, middle panel). The result is similar to GB09, such as early ToEs in northern-high latitude wettening regions and late ToEs in drying regions, although some regions have differences, such as earlier ToE in East Asia than GB09 (see below for details). ToEs tend to be earlier in greater radiative forcing scenarios and tend to be earlier in OM than in AS (Fig. 4). The signals in RCP2.6 are stable and weaker than in other RCPs (Figs. 2, 3), making ToEs delayed relative to other RCPs through mitigation. However, some regions, such as the northern high-latitude regions, East Asia, and drying regions except for the Mediterranean, have ToEs insensitive to the different scenarios. In contrast, other regions, such as SAS-AS, SAF-AS, and EAF-OM, have ToEs sensitive to the scenarios (Fig. 4).

Exact ToE years for each PSPOTs are displayed in Fig. 5, comparing results under three RCP scenarios. There are some regions showing considerable changes in ToEs according to different RCP scenarios, indicating that those regions could get benefit of reduced global warming through the ToE extension by taking lower emission scenarios. It is found that five out of 14 PSPOTs could experience ToE delay by at least 26 years if greenhouse-gas emission is reduced to RCP2.6 scenario levels, representing substantial benefits of emission reduction as Ciavarella et al. (2017) showed for extremely hot seasons.

3.3 ToE delay under mitigation

For more convenient comparisons, ToE delays are illustrated separately in Fig. 6. Red bars in Fig. 6 show ToE differences between RCP2.6 and RCP4.5 and blue bars indicate those between RCP2.6 and RCP8.5. Note that we neglect ToE differences with both ToEs occurring after 2080 (like the CAR-AS drying). The comparison of RCP2.6 with RCP4.5 scenario shows that ToEs are delayed in three PSPOTs—South Africa (drying, 59 years) and South Asia (wettening,

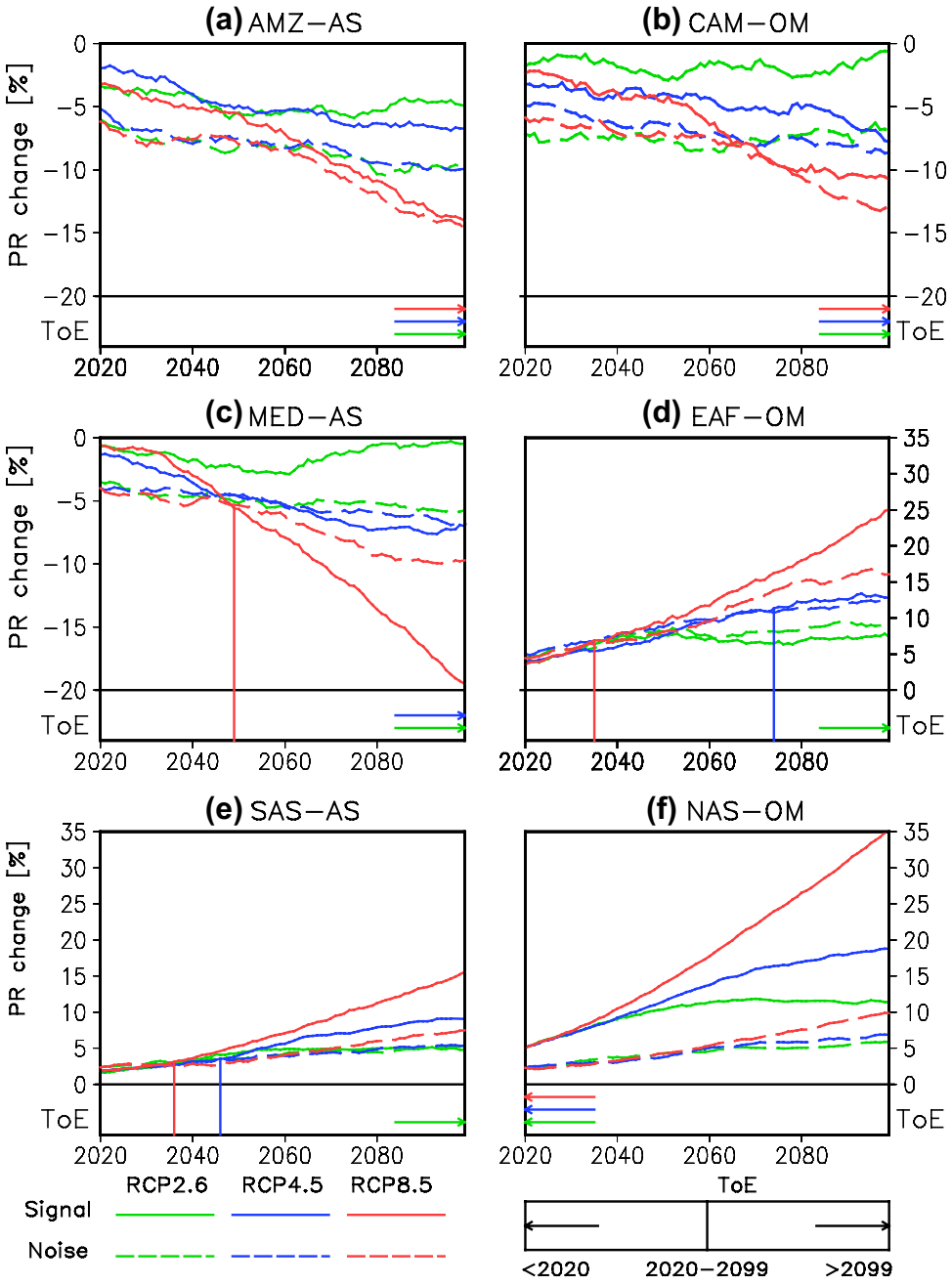

Fig. 3 Time evolution of precipitation change signal (20-year running mean, solid lines) and noise (dashed lines) over 6 PSPOTs and their corresponding ToEs in: AS season (AMZ, MED, and SAS) and OM season (CAM, EAF, and NAS) for RCP2.6, RCP4.5, and RCP8.5. For drying PSPOTs, negative signs are given to noise for better comparison

> 57 years) during AS, and over East Africa (wettening, > 26 years) during OM. When comparing RCP2.6 with RCP8.5, longer delays of ToEs occur in the three regions with South Asia (wettening, > 67 years), South Africa (drying, 62 years), and East Africa (wettening, > 66 years). Additionally, Mediterranean region is found to have ToE delays (drying, > 45 years) in both AS and OM seasons in the RCP2.6–RCP8.5 comparisons, suggesting that this region can be one of the regions with largest benefits.

Even when comparing RCP4.5 with RCP8.5, some regions might have benefits by the reduced emission of greenhouse gases, such as East Africa (OM) with a 40-year ToE delay, and the Mediterranean with more than a 45-year delay for both seasons (Fig. 7). It is notable that the differences in ToEs for different RCPs will be minor until the mid of the century due to similar radiative forcings. Indeed, SAS-AS and SAF-AS exhibit small differences in ToE between the RCP4.5 and RCP8.5 scenarios where both appear in the early twenty-first century (Fig. 7). This means that the ToEs will be similar between scenarios if both are early and that ToE differences can be only found for regions where the ToE occurs late.

As a whole, these results of ToE delays can be useful information for developing mitigation strategies for

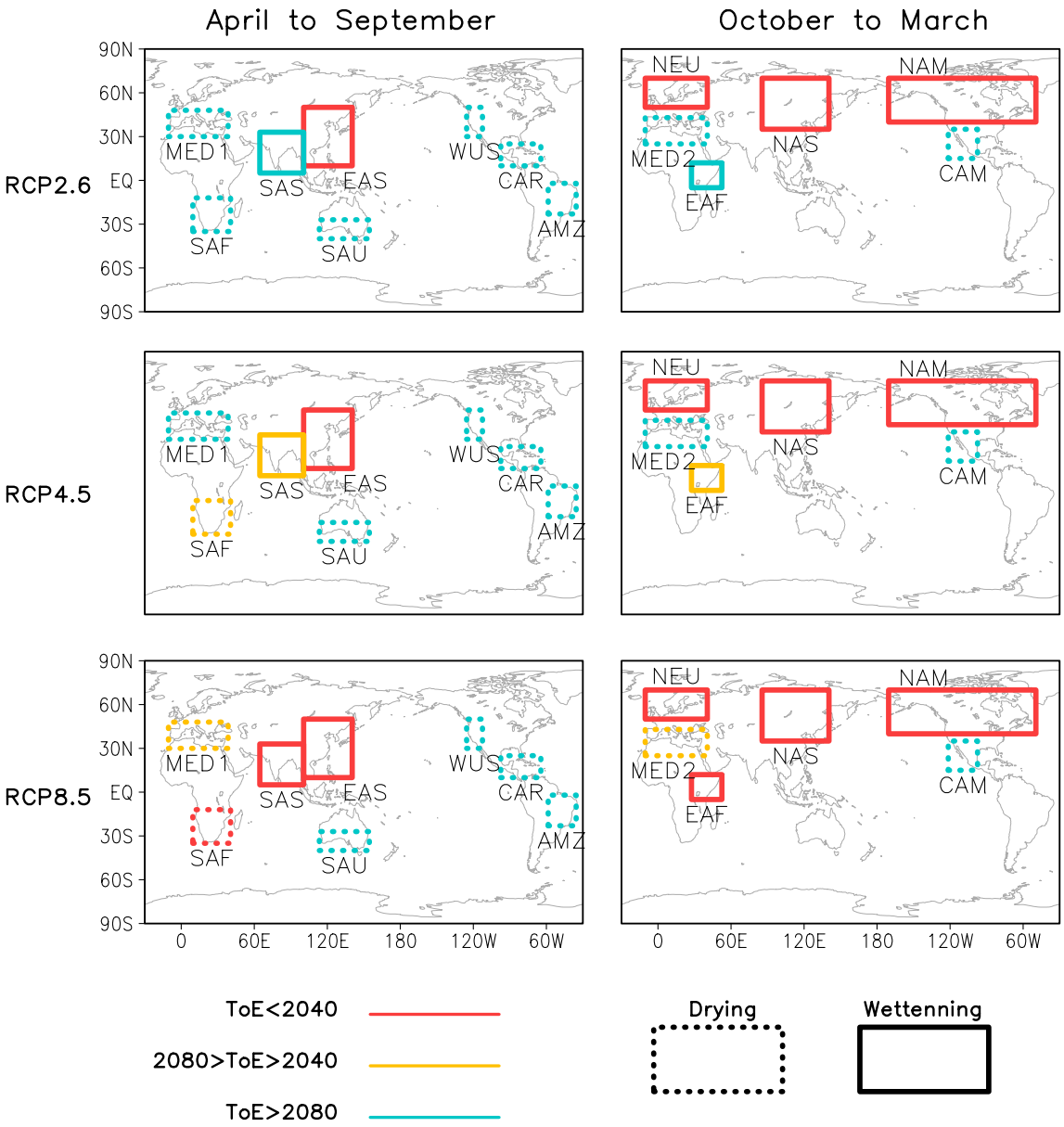

Fig. 4 Summary of ToEs (S/N > 1) over 14 PSPOTs in RCP2.6, RCP4.5, and RCP8.5 scenarios. Dashed and solid boxes represent drying and wettening trends, respectively. Red, yellow, and blue colors indicate ToE in the early (< 2040), mid (2040–2080), and late twenty-first century (> 2080), respectively

a given region, although the global nature of the RCPs should be considered with care. For example, in the Mediterranean in both seasons, by taking only RCP4.5 scenario rather than RCP8.5, the regions can get benefit from a ToE delay of 45 years. In contrast, for South Asia and South Africa, RCP2.6 should be considered more than RCP4.5 to postpone emergence (Figs. 6, 7).

3.4 ToE comparisons between CMIP3 and CMIP5

Overall, ToEs obtained from 28 CMIP5 models under RCP scenarios are similar to those in GB09, but some noticeable differences were observed in some PSPOTs such as East Asia, South Asia, and South Africa. This difference may be in part due to difference in models analyzed. In this respect,

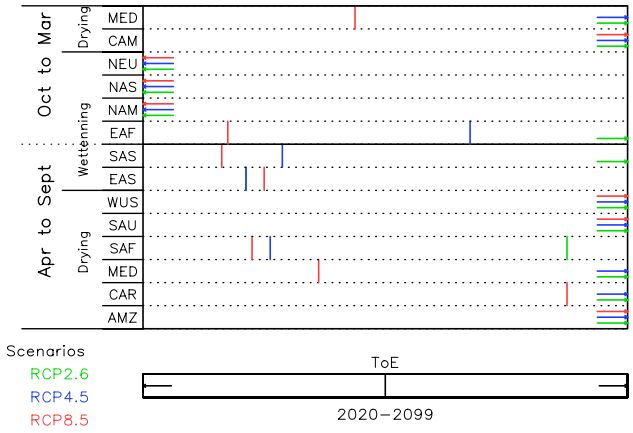

Fig. 5 ToE years (S/N > 1) over 14 PSPOTs obtained from RCP2.6 (green), RCP4.5 (blue), and RCP8.5 (red) scenarios. Left arrows indicate ToEs earlier than 2020 while right arrows depict ToEs later than 2099. Note that ToE for EAS-AS in RCP2.6 scenario is not shown, which is the same as that in RCP4.5 scenario

we explore the difference between CMIP3-based ToEs and CMIP5-based ToEs, by considering comparable scenario pairs: SRESA2 vs. RCP8.5, and SRESB1 vs. RCP4.5. It should be noted that the number of models is also different between GB09 and our study. The GB09 study used 14 CMIP3 models whereas we used 28 CMIP5 models. This difference in the number of sampled models may influence the difference in ToE years between our results and GB09. Therefore, for a fair comparison, we applied the same number of models by randomly selecting 14 out of 28 models and obtained ToEs. We repeated this procedure 1000 times and estimate 5–95% ranges of possible ToE ranges.

Figure 8 compares ToEs between CMIP3 and CMIP5 models for the SRESB1-RCP4.5 pairs. Box-whisker plots represent 5–95% ranges of ToEs estimated from 14 CMIP5 models. The random sampling provides larger ranges of CMIP5 ToEs in some regions like the Mediterranean (both seasons), East Africa, South Asia, and South Africa. However, these CMIP5 ranges include CMIP3-based ToEs, representing that CMIP5 ToEs are not inconsistent with CMIP3 ToEs in these regions. For example, the Mediterranean in AS exhibits different ToE between 28 CMIP5 models and 14 CMIP3 models, by about 40 years. However, ToE from SRESB1 is located within the 5–95% uncertainty range of ToEs from RCP4.5. Other regions with early ToEs before 2020 and late ToEs beyond 2080 show no difference in ToEs between CMIP3 and CMIP5 models, including the northern high-latitude regions (NEU-OM, NAS-OM, and NAM-OM) and some drying regions (WUS-AS and SAU-AS). East Asia and South Asia in AS are the only regions showing significant differences in ToE between the CMIP5 and CMIP3 models with about 10–20 years earlier ToEs in CMIP5 models compared to CMIP3 models.

When comparing ToE ranges in the RCP8.5 with those in the RCP4.5, ToEs of random groups under RCP8.5 have smaller uncertainty than ToEs of random groups under RCP4.5 over some regions (Fig. 9). This implies that the timing of signal emergence becomes more consistent among models under a stronger radiative forcing, which might be primarily due to the greater rate of change under RCP8.5 than RCP4.5. Thus, a larger difference is expected in ToE between CMIP3 and CMIP5 models in the RCP8.5 and SRESA2 scenario pairs (Fig. 9), but only two Asia monsoon PSPOTs and South Africa during AS exhibit a clear

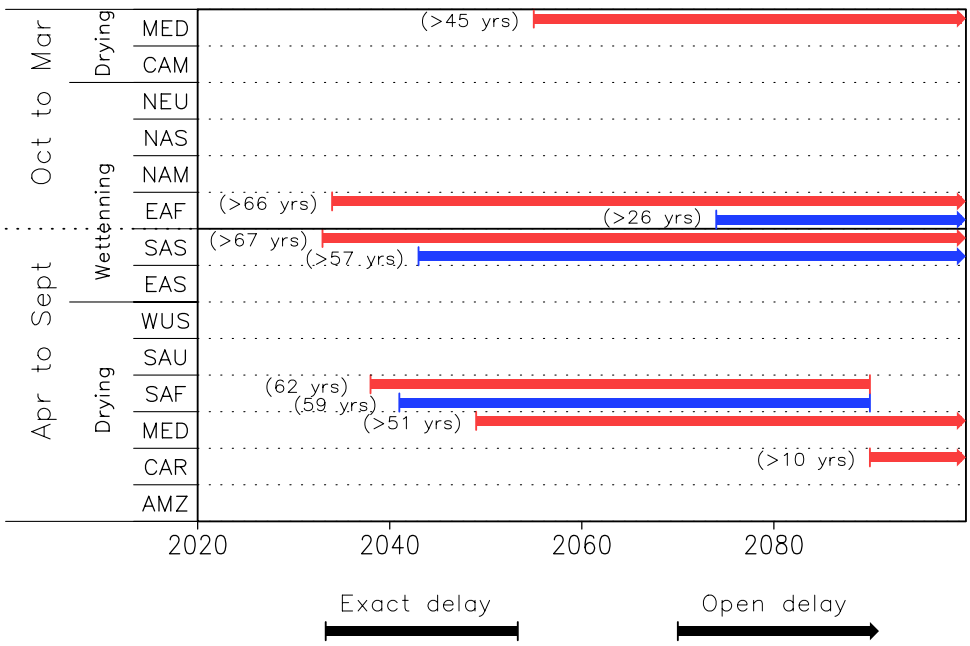

Fig. 6 ToEs (vertical line) and their difference (horizontal bars and arrows) between RCP2.6 and RCP4.5 (blue), and between RCP2.6 and RCP8.5 (red) over 14 PSPOTs. Exact and open delays of ToEs are illustrated below

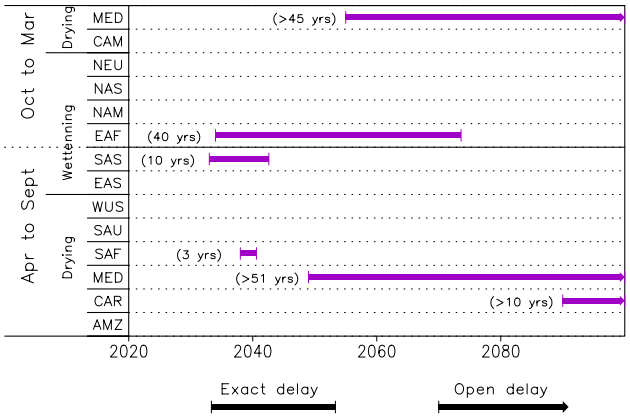

Fig. 7 Same as Fig. 6 but for comparing ToEs between RCP4.5 and RCP8.5

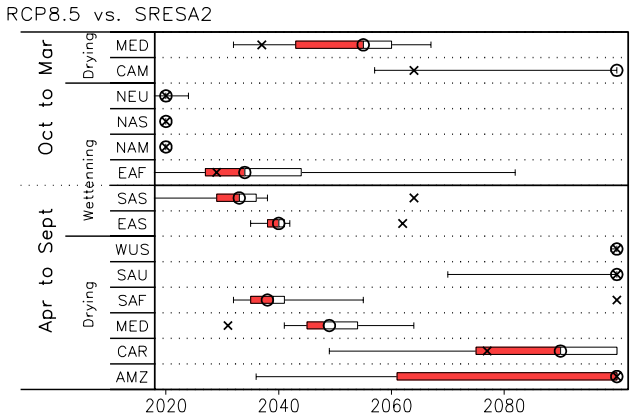

Fig. 9 Same as Fig. 8 but for CMIP3 SRESA2 scenario and CMIP5 RCP8.5 scenario

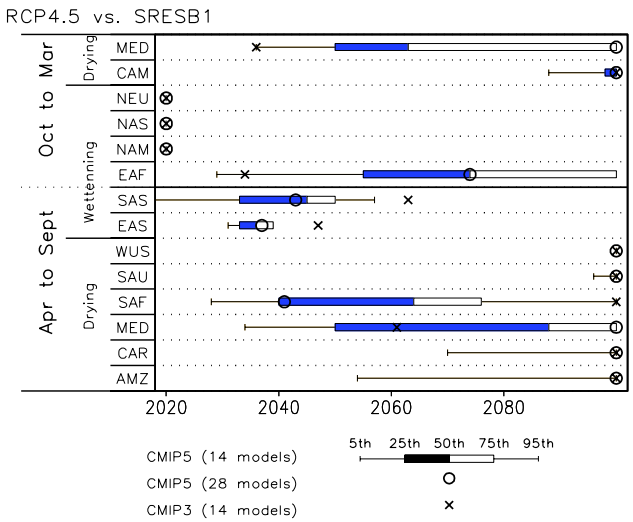

Fig. 8 Comparisons of ToEs over 14 PSPOTs between CMIP3 SRESB1 scenario (×mark) and CMIP5 RCP4.5 scenario (open circle). Horizontal box-whisker plots represent 5th to 95th percentile ranges of ToEs estimated from 14 randomly-selected CMIP5 models

difference in ToE, by at least 20 years, where CMIP3-based ToEs are completely outside of 5–95% uncertainty range of CMIP5-based ToEs.

We further investigated the ToE difference in these three regions (EAS, SAS, and SAF) by comparing the time series of signals and noise under the RCP8.5 and SRESA2 scenario pairs (Fig. 10). The results indicate that signals of precipitation changes are larger in CMIP5 than CMIP3, whereas difference in noise is not significant. For East Asia and South Asia, the signals from two CMIPs are not different until 2030 but after then about 3–4% difference appears and remains until the end of twenty-first century. Also, over South Africa, 5–10% difference in signals remains by the end of twenty-first century. Therefore, ToEs of these regions are earlier in CMIP5 than in CMIP3 due mainly to stronger signals. Results based on the RCP4.5-SRESB1 comparison support the stronger signal over these regions in CMIP5 (not shown).

The reasons why CMIP5 models have stronger signals in these regions remain unclear, warranting further in-depth investigations (Lee and Wang 2014). Here we have simply checked the possible influence of the model biases in present-day climatology. The inter-model correlations between future precipitation changes and precipitation climatology biases were found to be very low and insignificant for all three regions (not shown), suggesting that model bias may not be a dominant factor for CMIP3-CMIP5 difference in signal amplitudes, consistent with a previous work (Giorgi and Coppola 2010). We have also examined the inter-model relation between climate sensitivity (using TCR in Tables 1, 2) and precipitation change signal, which is found to be significant in the global mean results (Livia and Timothy 2014). In CMIP5 models, the relationship is unclear in South Asia and South Africa, while a significant correlation ($r = 0.41$) is seen over East Asia. In CMIP3, however, the results show no significant relationship. Precipitation change in East Asia in CMIP5 models seems to be more sensitive to radiative forcing than CMIP3 models, which might be related to the difference in implementation of aerosol effects, monsoon circulation, and/or influence of tropical oceans, which needs to be investigated in the future work (Lee and Wang 2014).

Signals will emerge earlier when using lower thresholds for signal-to-noise ratio. We tested sensitivity of ToEs to different S/N thresholds as $S/N > 0.5$ and $S/N > 2$ (not shown). Results suggested that some regions such as South Asia and South Africa in AS will experience earlier ToEs when using $S/N > 0.5$ and many regions have later ToEs at a more stringent threshold of $S/N > 2$, consistent with previous studies (Hawkins and Sutton 2012; Lee et al. 2016). This indicates a high sensitivity of ToEs to the S/N threshold, and one needs

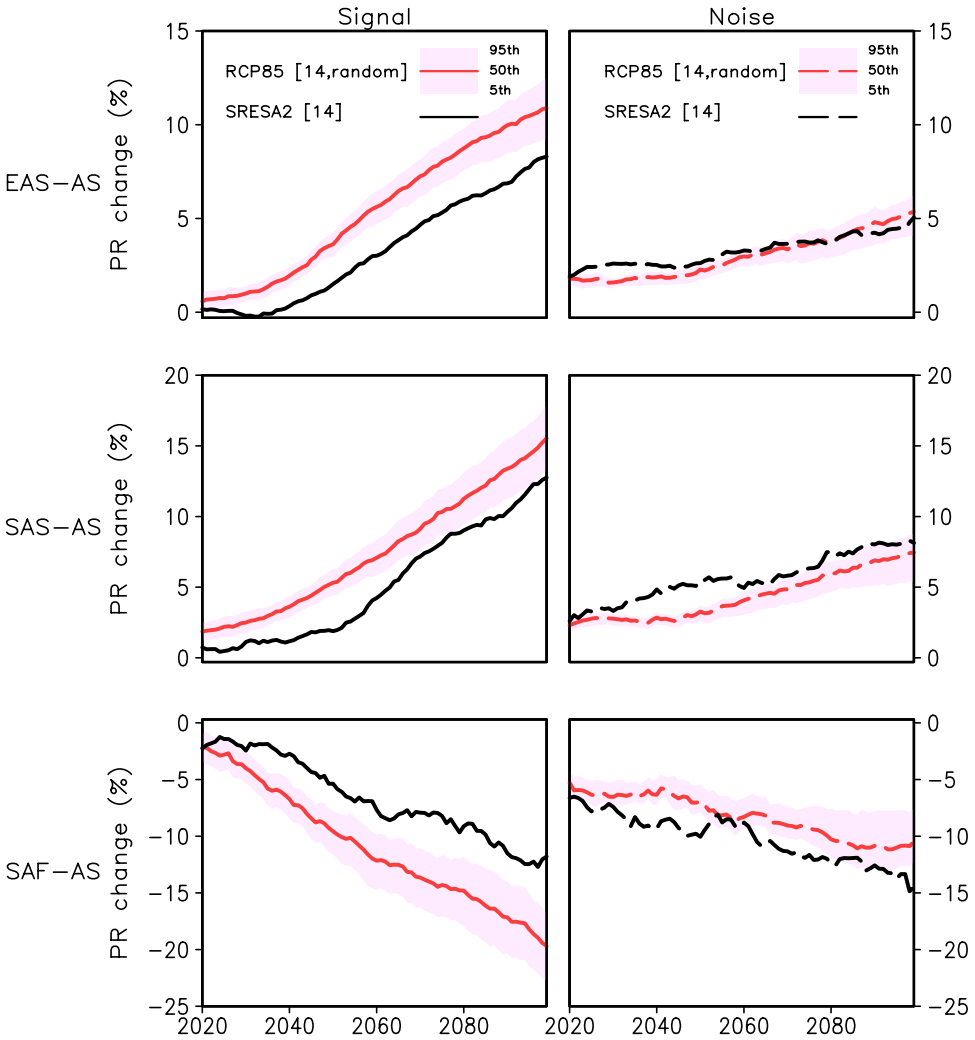

Fig. 10 Comparisons of time evolution of precipitation change signal (left) and noise (right) between CMIP5 RCP8.5 (red lines) and CMIP3 SRESA2 results (black lines) for East Asia, South Asia, South Africa during AS season. Red line and pink shading represents mean and 5–95% ranges estimated from 14 randomly-selected CMIP5 models

to choose it with care. We also tested the sensitivity of ToEs to using a 30-year moving window for estimating signals. The overall results are similar to the case of a 20-year moving window (not shown), suggesting insensitiveness of ToEs to the window interval.

4 Summary and discussion

In this study, we conducted an updated ToE analysis of regional precipitation changes during the twenty-first century by applying a signal-to-noise ratio method to multi-model datasets of CMIP5, simulated under three RCP scenarios. Following the previous study (GB09), we investigated ToEs over 14 precipitation change hotspots (PSPOTs) considering two seasons of April–September (AS) and October–March (OM), and found overall similar results. In addition, we examined possible ToE delays under mitigation by comparing those from a lower emission scenario (RCP2.6) with those from higher emission scenarios (RCP4.5 and RCP8.5). A few regions are identified with strong benefits of mitigation through ToE delays by 26 years and longer. The estimated ToE delay would be important information for strategy developers to mitigate the effects of climate change. To assess robustness of ToE results, we also examined the agreement in ToE between CMIP3 and CMIP5, for which the same numbers of models were considered for fair comparison. The main conclusions are summarized as follows, along with implications.

Results from RCP8.5 (high emission scenario) suggest that ToEs occur in the early twenty-first century over three northern high-latitude regions (OM wettening), East Africa (OM wettening), South Asia (AS wettening), East Asia (AS wettening) and South Africa (AS drying). The Mediterranean (both OM and AS drying) is expected to experience ToEs in the mid-twenty-first century (2040–2080). There will be no ToEs occurring in the twenty-first century in the other five region-season cases. The RCP2.6 scenario shows significantly later ToEs than RCP4.5 and RCP8.5 scenarios, with the delay

ranging from 26 to 67 years or longer over East Africa (OM wettening), the Mediterranean (both AS and OM drying), South Asia (AS wettening), and South Africa (AS wettening).

The ToE results from RCP4.5 are generally consistent with the results from SRESB1, and ToE results from RCP8.5 are also similar to the results from SRESA2, supporting the findings of GB09. In both cases, the similarity was greatest in the drying regions and northern high-latitude wettening regions. ToE comparisons between CMIP5 random-sampled models and CMIP3 models showed a considerable ToE difference of at least 20 years over East Asia, South Asia, and South Africa during AS in RCP8.5-SRESA2 comparisons, which was found to be due to a stronger signal in CMIP5 models than in CMIP3 models. ToE differences in these regions were largely insensitive to model precipitation bias or climate sensitivity. Some sensitivity tests indicated that ToEs will arrive earlier if a more stringent S/N threshold is used, consistent with previous studies. Using 30-year moving windows for signal definition provides similar ToEs as from 20-year moving windows, indicating a weak influence of the average period.

Estimates of ToE can be sensitive to the different definition of signal and noise, and two approaches have been developed and applied, one based on multi-model ensembles (MME, Christensen et al. 2007; GB09) and the other based on individual models (e.g., Hawkins and Sutton 2012; Maraun 2013; Sui et al. 2014). The ToE method based on individual model is based on the view of regarding internal variability as the only source of noise in the climate system (Maraun 2013), in which they estimate ToE from signal and noise defined from individual models and then measure ToE uncertainty considering inter-model differences in ToE. Although MME-based methods treat the inter-model difference as another source of 'projection' noise, the inter-model noise can arise from model errors related to different climate sensitivity as well as from internal variability, because model error and internal variability is difficult to disentangle due to a small number of simulations available for each model, particularly at regional scales (Deser et al. 2012; Kay et al. 2015). Therefore, although the two methods are based on different views, particularly in terms of noise definition (including or excluding inter-model uncertainties), both are appropriate and have been widely used to analyze signal emergence from noise. For the MME-based methods, Hawkins and Sutton (2011) analyzed the S/N in regional precipitation projections by applying a similar method to GB09 to the CMIP3 multi-model ensembles and identified the regions with relatively high S/N, which were largely consistent with the findings of GB09. Other studies applied GB09 method to assess ToEs of regional temperature and precipitation changes (Diffenbaugh and Scherer 2011; Diffenbaugh et al. 2011; Mariotti et al. 2015).

It is worth reconciling two ToE methods (although a comprehensive analysis is beyond the scope of this updated assessment), and we have conducted a sensitivity test using CMIP5 data (28 models listed in Table 1) by calculating ToEs from each model simulations and comparing the results with MME-based ones. For individual models, signal is defined as 20-year running means relative to the reference period (1980–1999) while noise is defined as a standard deviation of 20-year mean values, estimated from non-overlapping 20-year chunks of pre-industrial control simulations, following Hawkins and Sutton (2012) and Sui et al. (2014). Nine 20-year mean values from each model are used to make the sample size equal across models. Then, ToE is obtained for each model run by finding when the absolute value of signal is permanently greater than the noise. Figure 11 shows ToE results obtained from individual model runs for the three RCP scenarios. The inter-quantile ranges (IQR, 25th to 75th percentiles) of individual model ToE values show substantially large spread but in many hotspots, the IQR includes the ToE estimated from MME, indicating general agreement between two ToE methods. There are only a few cases with significant difference between two ToE estimates (i.e. MME ToE is beyond the IQR of individual model ToEs), including EAS for three RCPs and SAS for RCP8.5. Other than these exceptions, ToE estimated from MME tends to occur later than median ToE of individual model simulations, which is likely due to the larger noise level in GB09 method which contains inter-model uncertainty in the noise. We found that overall results are similar when using only the first run (r1i1p1) for each model to treat all of the models equally (not shown).

We note that some other factors may cause ToE uncertainty. Although we have considered this issue by random sampling (Figs. 8, 9), different studies assess ToEs or precipitation changes based on a differing number of models depending on their target regions, and model data availability. A different baseline period can produce different ToEs as well. We used 1980–1999, assuming that society has adapted to the current climate (King et al. 2015) and also for comparison to the previous GB09 study. A different choice of seasons, such as three or four months as relevant for each region, may be useful for impact assessment and adaptation planning.

Weather and climate extremes with high impacts on society have received more attention recently (SedláčekJ and Knutti 2014; Bador et al. 2016; King et al. 2016; Lehner et al. 2016; Lin et al. 2016; Schleussner et al. 2016) as hottest-recorded temperatures, droughts, and floods have appeared with higher frequency. Therefore, it is important to effectively inform policy makers and communities impacted on the benefits of greenhouse gas mitigation; regions that will gain benefits from ToE delay and types of extreme events. Also, other types of hotspots, identified based on the

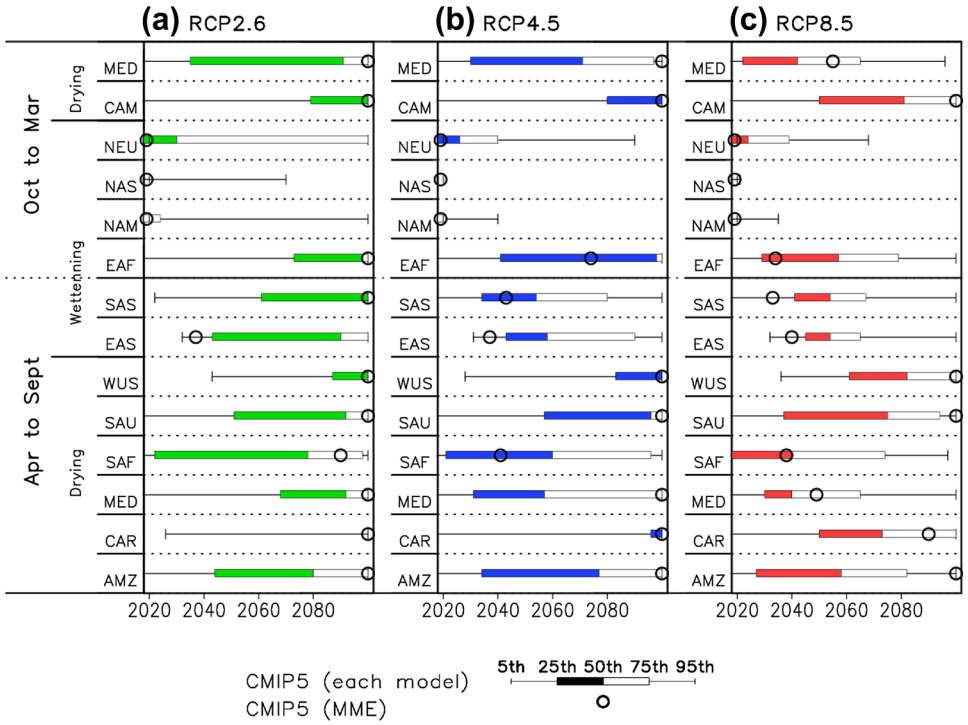

Fig. 11 Comparisons of ToEs over 14 PSPOTs from using multi-model mean (MME, open circle) and each model simulation (box-whisker) for RCP2.6, RCP4.5, and RCP8.5 scenarios. See text for details on how to estimate ToE from individual models

climate change impacts on environment and society (Hewitson et al. 2014), such as vulnerability or impact hotspots (Fraser et al. 2013; Piontek et al. 2014), need to be assessed as well.

Acknowledgements We thank two anonymous reviewers for their thoughtful comments. This work was supported by the National Research Foundation of Korea (NRF) grant funded by the Korea government (MEST) (no. 2017R1A2B2008951). We acknowledge the World Climate Research Programme's Working Group on Coupled Modelling, which is responsible for CMIP, and we thank the climate modeling groups (listed in Tables 1 and 2 of this paper) for producing and making available their model output.

References

Bador M, Terray L, Boé J (2016) Emergence of human influence on summer record-breaking temperatures over Europe. Geophys Res Lett 43:404–412

Bindoff NL et al (2013) Detection and attribution of climate change: from global to regional. In: Climate change 2013: the physical science basis. Contribution of working group I to the fifth assessment report of the intergovernmental panel on climate change, pp 869–928

Christensen JH et al (2007) Regional climate projections. In: Climate change the physical science basis. Contribution of working group I to the fourth assessment report of the intergovernmental panel on climate change, pp 849–926

Ciavarella A, Stott P, Lowe J (2017) Early benefits of mitigation in risk of regional climate extremes. Nat Clim Change 7:326–330

Collins M, Knutti R, Arblaset J et al (2013) Long-term climate change: projections, commitments and irreversibility. In: Stocker TF, Qin D, Plattner GK et al (eds) Climate change 2013: the physical science basis. Contribution of working group I to the fifth assessment report of the intergovernmental panel on climate change. Cambridge University Press, Cambridge

Dee DP et al (2011) The ERA-Interim reanalysis: configuration and performance of the data assimilation system. Q J R Meteorol Soc 137:553–597

Deser C, Phillips A, Bourdette V, Teng H (2012) Uncertainty in climate change projections: the role of internal variability. Clim Dyn 38:527–547

Diffenbaugh NS, Scherer M (2011) Observational and model evidence of global emergence of permanent, unprecedented heat in the 20th and 21st centuries. Clim Change 107:615–624

Diffenbaugh NS, Ashfaq M, Scherer M (2011) Transient regional climate change: analysis of the summer climate response in a high-resolution, century-scale ensemble experiment over the continental United States. J Geophys Res 116:D24111

Flato G et al (2013) Evaluation of climate models. In: Climate change 2013: The physical science basis. Contribution of working group I to the fifth assessment report of the intergovernmental panel on climate change, pp 743–824

Fraser EDG, Simelton E, Termansen M, Gosling SN, South A (2013) "Vulnerability hotspots": integrating socio-economic and hydrological models to identify where cereal production may decline in the future due to climate change induced drought. Agric For Meteorol 170:195–205

Giorgi F (2010) Uncertainties in climate change projections, from the global to the regional scale. EPJ Web Conf 9:115–129. https://doi.org/10.1051/epjconf/201009009

Giorgi F, Bi X (2009) Time of emergence (TOE) of GHG-forced precipitation change hot-spots. Geophys Res Lett 36:L06709

Giorgi F, Coppola E (2010) Does the model regional bias affect the projected regional climate change? An analysis of global model projections. Clim Change 100:787–795

Hawkins E, Sutton R (2011) The potential to narrow uncertainty in projections of regional precipitation change. Clim Dyn 37:407–418

Hawkins E, Sutton R (2012) Time of emergence of climate signals. Geophys Res Lett 39:L01702
Hawkins E, Anderson B, Diffenbaugh N, Mahlstein I, Betts R, Hegerl G, Joshi M, Knutti R, McNeall D, Solomon S, Sutton R (2014) Uncertainties in the timing of unprecedented climates. Nature 511:E3–E5
Herold N, Alexander LV, Donat MG, Contractor S, Becker A (2016) How much does it rain over land? Geophys Res Lett 43:341–348. https://doi.org/10.1002/2015GL066615
Hewitson B et al (2014) Regional context. In: Climate change 2014: impacts, adaptation, and vulnerability. Part B: regional aspects. Contribution of working group II to the fifth assessment report of the intergovernmental panel on climate change, pp 1133–1197
Kay JE et al (2015) The Community Earth System Model (CESM) large ensemble project: a community resource for studying climate change in the presence of internal climate variability. Bull Am Meteorol Soc 96:1333–1349
King AD, Donat MG, Fischer EM, Hawkins E, Alexander LV, Karoly DJ, Dittus AJ, Lewis SC, Perkins SE (2015) The timing of anthropogenic emergence in simulated climate extremes. Environ Res Lett 10:094015
King AD, Black MT, Min S-K, Fischer EM, Mitchell DM, Harrington LJ, Perkins-Kirkpatrick SE (2016) Emergence of heat extremes attributable to anthropogenic influences. Geophys Res Lett 43:3438–3443
Kirtman B et al (2013) Near-term climate change: projections and predictability. In: Climate change 2013: the physical science basis. Contribution of working group I to the fifth assessment report of the intergovernmental panel on climate change, pp 955–1008
Kjellström E, Bärring L, Nikulin G, Nilsson C, Persson G, Strandberg G (2016) Production and use of regional climate model projections—a Swedish perspective on building climate services. Clim Ser 2–3:15–29
Kuhlbrodt T, Gregory JM (2012) Ocean heat uptake and its consequences for the magnitude of sea level rise and climate change. Geophys Res Lett 39:L18608
Lambert SJ, Boer GJ (2001) CMIP1 evaluation and intercomparison of coupled climate models. Clim Dyn 17:83–106
Lee JY, Wang B (2014) Future change of global monsoon in the CMIP5. Clim Dyn 42:101–119
Lee D et al (2016) Time of emergence of anthropogenic warming signals in the Northeast Asia assessed from multi-regional climate models. Asia Pac J Atmos Sci 52:129–137
Lehner F, Deser C, Sanderson BM (2016) Future risk of record-breaking summer temperatures and its mitigation. Clim Change. https://doi.org/10.1007/s10584-016-1616-2
Lin L, Gettelman A, Fu Q, Xu Y (2016) Simulated differences in 21st century aridity due to different scenarios of greenhouse gases and aerosols. Clim Change. https://doi.org/10.1007/s10584-016-1615-3
Livia T, Timothy A (2014) The physical drivers of historical and 21st century global precipitation changes. Environ Res Lett 9:064024
Maraun D (2013) When will trends in European mean and heavy daily precipitation emerge? Environ Res Lett 8:014004
Mariotti A, Pan Y, Zeng N, Alessandri A (2015) Long-term climate change in the Mediterranean region in the mist of decadal variability. Clim Dyn 44:1437–1456
Min S-K, Park E-H, Kwon W-T (2004) Future projections of East Asian climate change from multi-AOGCM ensembles of IPCC SRES scenario simulations. J Meteorol Soc Jpn 82:1187–1211
Min S-K, Zhang X, Zwiers F (2008) Human-induced Arctic moistening. Science 320:518–520
Mora C et al (2013) The projected timing of climate departure from recent variability. Nature 502:183–187
Moss RH et al (2010) The next generation of scenarios for climate change research and assessment. Nature 463:747–756
Mullan D, Swindles G, Patterson T, Galloway J, Macumber A, Falck H, Crossley L, Chen J, Pisaric M (2016) Climate change and the long-term viability of the world's busiest heavy haul ice road. Theor Appl Climatol. https://doi.org/10.1007/s00704-016-1830-x
Muthers S et al (2014) The coupled atmosphere–chemistry–ocean model SOCOL-MPIOM. Geosci Model Dev 7:2157–2179
New M, Hulme M, Jones PD et al (2000) Representing twentieth century space–time climate variability. Part II: development of 1901–1996 monthly grids of terrestrial surface climate. J Clim 13:2217–2238
Noake K, Polson D, Hegerl G, Zhang X (2012) Changes in seasonal land precipitation during the latter twentieth-century. Geophys Res Lett 39:L03706
Peel MC, Finlayson BL, McMahon TA (2007) Updated world map of the Köppen–Geiger climate classification. Hydrol Earth Syst Sci 11:1633–1644
Phillips TJ, Gleckler PJ (2006) Evaluation of continental precipitation in 20th century climate simulations: the utility of multimodel statistics. Water Resour Res 42:W03202. https://doi.org/10.1029/2005WR004313
Piontek F et al (2014) Multisectoral climate impact hotspots in a warming world. Proc Natl Acad Sci 111:3233–3238
Räisänen J (2001) CO_2-induced climate change in CMIP2 experiments: quantification of agreement and role of internal variability. J Clim 14:2088–2104
Rogelj J, Meinshausen M, Knutti R (2012) Global warming under old and new scenarios using IPCC climate sensitivity range estimates. Nat Clim Change 2:248–253
Sarojini BB, Stott PA, Black E (2016) Detection and attribution of human influence on regional precipitation. Nat Clim Change 6:669–675
Schleussner CF et al (2016) Differential climate impacts for policy-relevant limits to global warming: the case of 1.5 °C and 2 °C. Earth Syst Dyn 7:327–351
Sedláček J, Knutti R (2014) Half of the world's population experience robust changes in the water cycle for a 2 °C warmer world. Environ Res Lett 9:044008
Stocker TF et al (2013) Technical summary. In: Climate change 2013: the physical science basis. Contribution of working group I to the fifth assessment report of the intergovernmental panel on climate change, pp 35–109
Sui Y, Lang X, Jiang D (2014) Time of emergence of climate signals over China under the RCP4.5 scenario. Clim Change 125:265–276
van Vuuren DP et al (2011) The representative concentration pathways: an overview. Clim Change 109:5–31
Wan H, Zhang X, Zwiers F, Min S-K (2015) Attributing northern high-latitude precipitation change over the period 1966–2005 to human influence. Clim Dyn 45:1713–1726